

# A Simplified Model for the Forced Libration of Icy Moons with Subsurface Oceans: Application to Enceladus and Mimas

Yeva Gevorgyan,<sup>1</sup>\*

<sup>1</sup>CEMSE Division, King Abdullah University of Science and Technology, Thuwal 23955-6900, Saudi Arabia.

Accepted XXX. Received YYY; in original form ZZZ

## ABSTRACT

In this work, we investigate a minimalist model capable of accurately replicating the forced librations of an icy moon with a subsurface ocean. The model holds potential to predict the presence of a subsurface ocean through analysis of longitudinal librations. We demonstrate that a two-layered model, with a prestressed icy crust and a fixed mantle cavity, can effectively model the librational behavior of icy moons. The proposed model is applied to model the longitudinal libration of Enceladus and Mimas, two medium-sized icy moons of Saturn.

**Key words:** planets and satellites: interiors – planets and satellites: oceans – planets and satellites: composition

## 1 INTRODUCTION

Deciphering the internal structure and composition of moons and planets within our Solar System holds the key to exploring their astrobiological potential and is one of the top goals of modern planetary science. There is considerable evidence for the existence of subsurface oceans in the icy moons of the Jovian and Saturnian systems, e.g. Titan, Enceladus, Mimas, Europa, Ganymede, and Callisto (Nimmo & Pappalardo 2016). Liquid water is a key ingredient for the formation of life as we know it, and evidence of stable liquid water elsewhere could indicate an environment beyond Earth that could sustain life. (Vance et al. 2018).

In the absence of direct *in-situ* geophysical measurements, which are currently limited to Earth (Dziewonski & Anderson 1981; Tromp 2020), the Moon (Khan et al. 2013; Matsumoto et al. 2015; Garcia et al. 2019), and Mars (Khan et al. 2021), an alternative indirect approach to understanding the interior composition of celestial bodies involves investigating the global-scale geophysical data obtained from orbiting spacecraft, e.g. mass, mean moment of inertia and tidal response (Bagheri et al. 2022).

Many of the Solar System moons are in a synchronous rotation state performing tidally-induced tiny oscillations, caused by non-spherical mass distributions and eccentric orbits. These oscillations are known as librations (Figure 1 illustrates the tidal mechanism acting between a planet (Saturn) and its moon (Enceladus)) and their amplitude remains one of the few measurable parameters for distant moons and planets. The libration amplitude encodes critical information on the internal structure of the body (Gevorgyan et al. 2020; Ragazzo et al. 2022) that can help to detect global subsurface oceans (Thomas et al. 2016) and structure, in general (Rambaux et al. 2012; Dmitrovskii et al. 2022). Considering simple and accurate models for the librations is especially important in the era of big data, where efficient analysis is crucial.

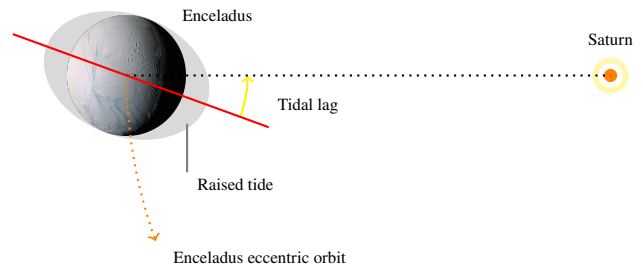


**Figure 1.** Illustration of the tidal action between a planet (Saturn) and its moon (Enceladus). Enceladus moves on a synchronized elliptical orbit, which makes its instantaneous orbital speed vary. At its closest point to Saturn, Enceladus rotates slower than it orbits, so the raised tide lies slightly behind the Enceladus-Saturn (dashed) line in the direction of Enceladus’s rotation. At its most distant point to Saturn, the opposite is true. As a result, the raised tide performs tiny oscillations called librations.

The measurement of libration amplitude relies on surface image processing (Thomas et al. 2016; Nadezhdina et al. 2016; Tajeddine et al. 2014). The observed librations are that of the external shell of the body. The outer shell can either overlay a global subsurface liquid layer while being mechanically detached from the rest of the body, or be at least partially connected with the interior. Third possibility is an outer shell overlying a liquid core. Schematic illustration of the three cases can be seen in Figure 2. To accurately replicate the libration motions of a mechanically detached shell, a model with at least two layers is needed. This model can consist of a deformable crust overlying an effective liquid layer, as described by (Ragazzo et al. 2022). Alternatively, for bodies with no mechanical detachment the response to the libration raising torque depends on the moment of inertia of the whole body (Tiscareno et al. 2009), and an effective rheological model can aptly reproduce their librations (Gevorgyan et al. 2020).

In this work we model forced longitudinal librations using a two

\* E-mail: yeva.gevorgyan@kaust.edu.sa

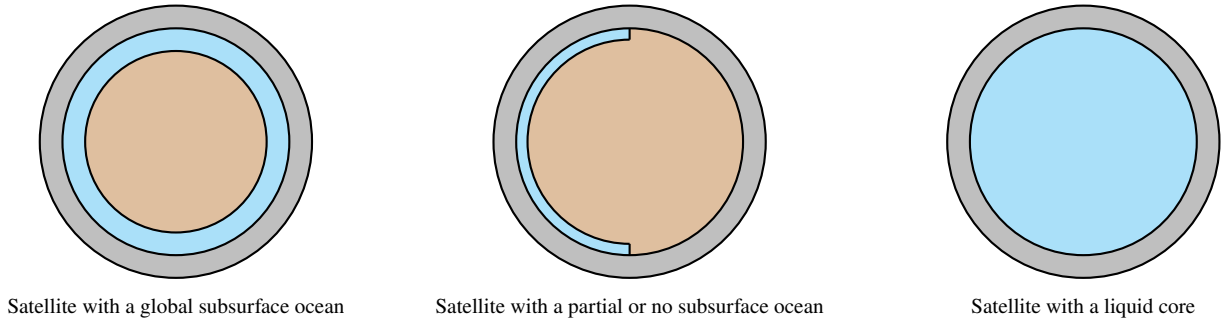


**Figure 2.** Three possible internal structures for icy satellites.

layered rheological model first introduced in (Ragazzo et al. 2022). We show that with this model we can reproduce the measured longitudinal librations of icy moons, for a reasonable range of body parameters. We compare librations of the mantle to that of the effective body to gain insight on core mantle mechanical decoupling. Note that a core mantle decoupling can either decrease or increase the libration amplitude, depending on the shell thickness and rigidity (Jara-Oru e & Vermeersen 2014). There are a few bodies in the Solar System for which the forced libration amplitude was measured: Enceladus Thomas et al. (2016); Nadezhdina et al. (2016), Dione Beuthe et al. (2016), Europa, Ganymede, Callisto Rambaux et al. (2011), and Mimas (Tajeddine et al. 2014). Here we will illustrate our results by modelling forced librations of two similarly sized moons of Saturn, Enceladus and Mimas. For the reference we also investigate energy dissipation rate in the viscoelastic crust and core mantle boundary of the moons.

The paper is structured as follows: In Section 2, we shortly discuss the rheological models, model parameters and initial conditions used in the paper. In Section 3 we present concrete application to the moons and discuss the range of body parameters. In Section 4 we present and analyze the results. Finally, in the Section 5, we summarize the main results and discuss the implications of our findings.

## 2 DYNAMICAL MODEL

### 2.1 Solid-fluid model

We consider a two-layered viscoelastic rheological model, introduced in (Ragazzo et al. 2022), for the interior of a stratified celestial body. The model comprises two layers: an outer shell lying over an effective fluid core. The shell is viscoelastic, prestressed, and is allowed to slide over the fluid layer, and represents the actual crust-mantle of the body. The core mantle boundary (CMB) is assumed to move as a rigid, spherically symmetric surface. The fluid core is an effective representation of the rest of the body; it can either be the actual liquid core of the body or a composition of the subsurface ocean and the solid core. Here we do not consider further stratification of each layer. The model allows to predict the forced longitudinal librations of the mantle, which can be directly compared with the observed librations of the body. We also can follow the librations of the mean body by looking at rotation of its Tisserand frame. Tisserand frame is defined as the body frame in which total angular momentum is zero at all times. The frame behaves as the mean body, hence its libration can be interpreted as libration of the average body. The amplitude of this libration is equivalent to the amplitude of libration that we would

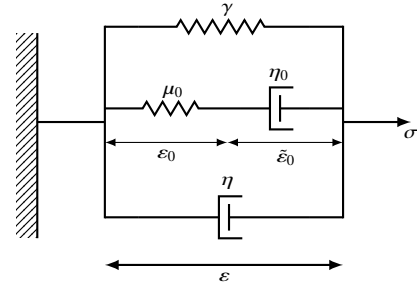


**Figure 3.** Mantle rheological model. The spring  $\gamma$  represents the effect of gravity. The damper  $\eta$  and the Maxwell element ( $\mu_0$ ,  $\eta_0$ ) represent the effect of the macroscopic (spatial average) rheology of the mantle;  $\varepsilon$ ,  $\varepsilon_0$  and  $\tilde{\varepsilon}_0$  denote strains and  $\sigma$  the stress.

obtain with an effective homogeneous rheology as in (Gevorgyan et al. 2020).

#### 2.1.1 The equations of motion

The equations of motion for a two layered, extended, deformable body, for example an icy satellite, evolving under the influence of the host planet, a point mass, are described below. Let  $\kappa = (\mathbf{i}, \mathbf{j}, \mathbf{k})$  be an inertial reference frame at the centre of mass of the extended body. The Lagrangian of rotation of the deformable body is

$$\mathcal{L}_{\text{ROT}} = \frac{1}{2} \omega_m \cdot \mathbf{I}_m \omega_m + \frac{1}{2} \omega_c \cdot \mathbf{I}_c \omega_c - \frac{3}{2} \frac{\mathcal{G}M}{r^5} \mathbf{r} \cdot \mathbf{I}_T \mathbf{r}, \quad (1)$$

where  $\omega_\alpha$  is the angular velocity of the layer  $\alpha$  ( $\alpha$  is replaced by  $m$  for the mantle, by  $c$  for the core, and by  $T$  for the entire body) with respect to an inertial frame  $\kappa$  and  $\mathbf{I}_\alpha$  the matrix of inertia also written in the same inertial frame,  $M$  is the mass of the point mass,  $r$  is the position of the point mass in  $\kappa$ , and  $\mathcal{G} = 6.6743 \times 10^{-11} \text{ m}^3 \cdot \text{kg}^{-1} \cdot \text{s}^{-2}$  is the gravitational constant.

To model the deformation of the body we assign a macroscopic rheological model in Figure 3 to the mantle. The spring of rigidity  $\gamma$  represents the gravity, a dash-pot of viscosity  $\eta$  accounts for the dissipation, and a Maxwell element with elasticity and viscosity ( $\mu_0$ ,  $\eta_0$ ), which under the condition  $\eta_0 \ll \eta$  allows the existence of a prestress in the model. The Association Principle in (Ragazzo & Ruiz 2017) is applied to obtain the deformation Lagrangian

$$\mathcal{L}_{\text{TID}} = \frac{1}{2} \gamma \mathbf{I}_{\sigma, T} \|\mathbf{B}_T\|^2 - \frac{1}{2} \mu_0 \mathbf{I}_{\sigma, T} \|\mathbf{B}_T - \mathbf{B}_0\|^2, \quad (2)$$

where  $\mathbf{B}_\alpha$  are the deformation matrices, satisfying  $\mathbf{I}_\alpha = \mathbf{I}_{\sigma, \alpha} (\mathbb{I} - \mathbf{B}_\alpha)$ , with  $\mathbf{I}_{\sigma, \alpha} = \frac{1}{3} \text{Tr}(\mathbf{I}_\alpha)$  being the mean moment of inertia and  $\mathbf{B}_0$  the

fossil-deformation matrix. The elastic stress within the mantle at the equilibrium state is represented by the prestress  $\mu_0(\mathbf{B}_T - \mathbf{B}_0)$ . The prestress allows to build a mathematical model to describe the librations of slightly aspherical bodies out of hydrostatic equilibrium and its importance is discussed in (Ragazzo et al. 2022). To model the non-conservative forces we have to add the Rayleigh dissipation function to the Lagrangian

$$\mathcal{D} = \frac{1}{2}\eta\mathbf{I}_{o,T}\|\dot{\mathbf{B}}_T - [\widehat{\omega}_m, \mathbf{B}_T]\|^2 + \frac{1}{2}k_c\|\omega_m - \omega_c\|^2, \quad (3)$$

where  $\widehat{\omega}_\alpha$  is an anti-symmetric operator of rotation,<sup>1</sup> and  $k_c$  is a core-mantle boundary coupling constant.

The equations of motion in the inertial frame obtained with Poincaré-Lagrange formalism are

$$\begin{aligned} \dot{\pi}_m &= \mathbf{I}_c\omega_c \times \omega_c - k_c(\omega_m - \omega_c) - 3\frac{\mathcal{G}M}{r^5}(\mathbf{I}_T\mathbf{r}) \times \mathbf{r} \\ \dot{\pi}_c &= \omega_c \times \mathbf{I}_c\omega_c + k_c(\omega_m - \omega_c) \\ \eta\dot{\mathbf{B}}_T &= \eta[\widehat{\omega}_m, \mathbf{B}_T] - \gamma\mathbf{B}_T - \mu_0(\mathbf{B}_T - \mathbf{B}_0) + \mathbf{F} \\ \dot{\mathbf{B}}_c &= [\widehat{\omega}_m, \mathbf{B}_c] \\ \dot{\mathbf{B}}_0 &= [\widehat{\omega}_m, \mathbf{B}_0], \end{aligned} \quad (4)$$

where

$$\begin{aligned} \mathbf{F} &= -\left(\omega_m \otimes \omega_m - \frac{\omega_m^2}{3}\mathbb{I}\right) + 3\frac{\mathcal{G}M}{r^5}\left(\mathbf{r} \otimes \mathbf{r} - \frac{r^2}{3}\mathbb{I}\right) \\ \mathbf{B}_m &= (\mathbf{I}_{o,T}\mathbf{B}_T - \mathbf{I}_{o,c}\mathbf{B}_c)/\mathbf{I}_{o,m} \\ \omega_T &= \mathbf{I}_T^{-1}\mathbf{I}_m\omega_m + \mathbf{I}_T^{-1}\mathbf{I}_c\omega_c = \omega_m + \mathbf{I}_T^{-1}\mathbf{I}_c(\omega_c - \omega_m) \\ \omega_m &= \mathbf{I}_m^{-1}\pi_m \\ \omega_c &= \mathbf{I}_c^{-1}\pi_c \\ \mathbf{I}_T &= \mathbf{I}_m + \mathbf{I}_c. \end{aligned} \quad (5)$$

To have the complete set of equations to integrate the two body system we need to add the equations for the position and the velocity of the extended body. To keep the extended body on an eccentric orbit and to attain the forced oscillations regime we fix the eccentricity and the semi-major axis at the present values and remove tidal evolution from the orbits. For the sake of simplicity, no obliquity is taken into consideration in this manuscript.<sup>2</sup> In the inertial frame the remaining equations of motion are (Gevorgyan et al. 2020)

$$\begin{aligned} \dot{\mathbf{r}} &= \mathbf{v} \\ \dot{\mathbf{v}} &= -\mathcal{G}(M + m_1)\frac{1}{r^3}\mathbf{r}. \end{aligned} \quad (6)$$

In the next section we show the relation of the the model parameters to potentially observable quantities.

<sup>1</sup> To every vector  $x \in \mathbb{R}^3$  we associate an anti-symmetric operator by means of the hat operator defined as

$$x = \begin{pmatrix} x_1 \\ x_2 \\ x_3 \end{pmatrix} \in \mathbb{R}^3 \mapsto \widehat{x} = \begin{bmatrix} 0 & -x_3 & x_2 \\ x_3 & 0 & -x_1 \\ -x_2 & x_1 & 0 \end{bmatrix} \in \text{skew}(3).$$

<sup>2</sup> Note that the obliquity can be easily added and treated in the framework of our model if necessary, as can be seen in (Ragazzo et al. 2022).

### 2.1.2 Model parameters

We establish a connection between the parameters of the present model and the ones measured or estimated for the celestial bodies. The rigidity  $\gamma$  of the gravitation spring in Figure 3 is estimated from

$$\gamma = \frac{4}{5}\frac{\mathcal{G}m_1}{R_I^3}, \quad R_I = \sqrt{\frac{5\mathbf{I}_{o,T}}{2m_1}}, \quad (7)$$

where  $R_I$  is the inertial radius. This expression was derived by Ragazzo (2020). Core-mantle boundary (CMB) coupling constant, responsible for the dissipation at the boundary, can not be estimated from the observations, except in very few cases like for the Moon. Theoretical method used in (Peale et al. 2014) for Mercury can be used to estimate the constant. The authors use fluid dynamic arguments to arrive at the equation

$$k_c = \nu\frac{1}{R_c^2}\frac{\mathbf{I}_{o,c}\mathbf{I}_{o,m}}{\mathbf{I}_{o,T}}, \quad (8)$$

where  $R_c$  is the mean radius of the core and  $\nu$  is the kinematic viscosity of the fluid in the core. In (Ragazzo et al. 2022, section 3.4) authors discuss in detail how to obtain  $k_c$  from CMB and core fluid physical characteristics, and why the kinematic viscosity can be replaced by the eddy-viscosity of the fluid.

Mean moments of inertia of the mantle, core and the entire body are related to gravitational coefficients of the satellites as

$$\begin{aligned} \frac{\mathbf{I}_{o,T}}{MR_T^2} &= \frac{C_T}{MR_T^2} + \frac{2}{3}C_{20T} \\ \frac{\mathbf{I}_{o,c}}{MR_T^2} &= \frac{C_c}{MR_T^2} + \frac{2}{3}C_{20c} \\ \frac{\mathbf{I}_{o,m}}{MR_T^2} &= \frac{\mathbf{I}_{o,T}}{MR_T^2} - \frac{\mathbf{I}_{o,c}}{MR_T^2}, \end{aligned} \quad (9)$$

where  $C_{20\alpha}$  are gravity fields and  $\frac{C_T}{MR_T^2}$  are polar moments of inertia.

The prestress-elastic constant can be estimated if we know the potential Love number and mean moment of inertia of the body, and is not directly related to the viscosity of the mantle. The constant is estimated as

$$\mu_0 = 3\frac{\mathcal{G}(M + m_1)}{1 + M/m_1}\frac{\mathbf{I}_{o,T}}{MR_T^2}\frac{1}{R_T^3k_2} \quad (10)$$

where  $k_2$  is the potential Love number of the deformable body.

## 2.2 Initial conditions and integration of the model

In this section we specify the initial conditions for some keynote variables necessary to initiate the integration of the equations of motion. The fossil deformation matrix should be initialized with well estimated theoretical or experimental values since it does not change through the integration and plays a crucial role then modelling longitudinal librations. Above mentioned matrix is evaluated from the mean moments of inertia of the extended body as

$$\begin{aligned} \mathbf{B}_0(0) &= \frac{2}{3}\frac{MR_T^2}{\mathbf{I}_{o,T}} \begin{bmatrix} 3C_{22T} - \frac{1}{2}C_{20T} & 0 & 0 \\ 0 & -3C_{22T} - \frac{1}{2}C_{20T} & 0 \\ 0 & 0 & C_{20T} \end{bmatrix} \\ &+ \frac{n^2}{3\mu_0} \begin{bmatrix} -1 & 0 & 0 \\ 0 & -1 & 0 \\ 0 & 0 & 2 \end{bmatrix}. \end{aligned} \quad (11)$$

The initial value for the deformation of the core is estimated from its moments of inertia as

$$\mathbf{B}_c(0) = \frac{2}{3} \frac{M\mathcal{R}_T^2}{I_{o,c}} \begin{bmatrix} -\frac{1}{2}C_{20c} & 0 & 0 \\ 0 & -\frac{1}{2}C_{20c} & 0 \\ 0 & 0 & C_{20c} \end{bmatrix}. \quad (12)$$

The orbit and the rotation of the system can be set to their current values. The deformation matrix of the entire body can be initialized as described in (Ragazzo & Ruiz 2017; Gevorgyan et al. 2020).

The numerical integration of the system of first order ODEs in (4) and (6) is carried by a Runge-Kutta method of order 8 with embedded error estimator of order 7 due to Dormand & Prince, with step size control (Hairer et al. 1993).

### 3 APPLICATIONS: ENCELADUS AND MIMAS

We choose Enceladus and Mimas, two medium sized moons of Saturn, to test our model. The moons are similar in size and are orbiting Saturn on neighbouring orbits, yet the observer encounters two very different surface patterns. The surface difference suggests different internal structure and maybe different formation and evolution mechanisms. The amplitude of forced longitudinal libration, we are interested in here, was estimated for both Enceladus (Thomas et al. 2016; Nadezhdina et al. 2016) and Mimas (Tajeddine et al. 2014) from Cassini mission data. Enceladus, likely, has a global subsurface ocean (Thomas et al. 2016), supported by longitudinal libration amplitude and the presence of south polar plumes. Unusually high measured libration amplitude of Mimas can be explained either with the presence of a global subsurface ocean or by a non-hydrostatic core (Tajeddine et al. 2014). We consider both Enceladus and Mimas with global subsurface ocean, their schematic internal structure can be seen on the far left in Figure 2. The goal here is to model the longitudinal librations of these two bodies using the two-layered model introduced in the previous section, namely a two-layered body with an icy crust and an effective liquid core. The host planet, Saturn, is considered to be a point mass raising tides on Enceladus and Mimas. The mass of Saturn is taken from NASA Planetary Fact Sheets and is  $5.683 \times 10^{26}$  kg. Present physical and orbital parameters of the moons are provided in Table 1. We consider a wide range of model parameters, such as shell thickness, rigidity, and viscosity of the mantle, to obtain the range that best fits the observations of longitudinal libration amplitude.

#### 3.1 Enceladus interior model

Enceladus orbits Saturn on a synchronised, slightly eccentric orbit, sustained by mean motion resonance with Dion, yet another moon of Saturn. There are two estimates for the longitudinal libration amplitude of Enceladus from Cassini data:  $0.^\circ 120 \pm 0.^\circ 014$  (Thomas et al. 2016) and  $0.^\circ 155 \pm 0.^\circ 014$  (Nadezhdina et al. 2016).

Below we present set of parameters we considered for the interior of Enceladus. The density of Enceladus's icy crust is fixed at  $850 \text{ kg/m}^3$ , a value widely used in the literature. We test ice shell thicknesses in the range from 2 to 60 km to evaluate the dependence of the libration amplitude on the ice thicknesses in our model and to find the thickness that best fits the observed libration amplitude. We consider three values for the prestress elasticity constant 0.27 GPa, 0.54 GPa, 1.08 GPa, which are equivalent to potential Love number of 0.0055, 0.011, 0.022, respectively. The values are within the uncertainty interval for the potential Love number estimated in (Ermakov et al. 2021). The viscosity of the ice shell is tested in

**Table 1.** Present day physical and orbital parameters of Enceladus and Mimas

	Enceladus	Mimas
$m_1$	$1.08 \times 10^{20}$ kg	$0.379 \times 10^{20}$ kg
$R$	$252.1 \times 10^3$ m	$198.66 \times 10^3$ m
$e$	0.0045	0.0202
$a$	$2.38 \times 10^8$ m	$1.8552 \times 10^8$ m
$n$	$5.308 \times 10^{-5}$ rad · s <sup>-1</sup>	$7.716 \times 10^{-5}$ rad · s <sup>-1</sup>
$I_{o,T}$	$2.2994 \times 10^{30}$ kg · m <sup>2</sup>	$5.57187 \times 10^{29}$ kg · m <sup>2</sup>
$I_{oT}/M\mathcal{R}_T^2$	0.335	0.375
$C_T/M\mathcal{R}_T^2$	0.3386	0.385
$C_{20T}$	$-5.4352 \times 10^{-3}$	$-1.5 \times 10^{-2}$
$C_{22T}$	$1.5498 \times 10^{-3}$	$3.6 \times 10^{-3}$
$\gamma$	$4.69504 \times 10^{-7}$ s <sup>-2</sup>	$7.33073 \times 10^{-7}$ s <sup>-2</sup>
$\nu$	$0.3 \text{ m}^2 \cdot \text{s}^{-1}$	$0.3 \text{ m}^2 \cdot \text{s}^{-1}$
$k_2$	$0.0167^{+0.0403}_{-0.0119}$	0.01

Masses, radii, eccentricities, semi-major axis, and rotation rate of both moons are taken from NASA Planetary Fact Sheets. The rigidity constant  $\gamma$  is calculated for both bodies using the method in (Correia et al. 2018).

Gravitational coefficients  $C_{20T}$ ,  $C_{22T}$  and total moment of inertia of Enceladus were taken from (Iess et al. 2014). Mean moment of inertia of Mimas is taken from (Gyalay & Nimmo 2022), and the gravitational coefficients are estimated. Estimate of eddy viscosity  $\nu$  of the fluid inside Enceladus core is taken from (Kang et al. 2022), the same eddy viscosity is used for the ocean of Mimas. Potential Love number  $k_2$  of Enceladus taken from (Ermakov et al. 2021), and of Mimas from (Lainey et al. 2024).

the interval of  $10^{12} - 10^{17}$  Pa · s, usually accepted in the literature (Běhounková et al. 2015; Efromisky 2018; Gevorgyan et al. 2020). Core moments of inertia are varied linearly with the size of the core.

#### 3.2 Mimas interior model

Mimas orbits Saturn on a much more eccentric synchronised orbit than Enceladus. The source of anomalously large current day eccentricity of Mimas is not clear. The longitudinal libration amplitude of Mimas estimated from Cassini data is  $0.^\circ 8383 \pm 0.^\circ 017$  (Tajeddine et al. 2014). Flattening of Mimas shell plays an important role while modelling its forced longitudinal librations (Lainey et al. 2024). Moreover, Mimas is in the limit of size and mass to achieve hydrostatic equilibrium and its likely that prestress plays an important role in the libration model. The prestress in our model is calculated from Equation (11) and depends mainly on the gravitational coefficients of first order, namely  $J_2$  and  $C_{22}$ . For Mimas there are no observational constraints for the gravitational coefficients, hence this parameters are adjusted here to obtain the observed libration amplitude. Gravitational coefficients estimated in (Lainey et al. 2024) were used as reference. The density of the crust is assumed to be the same as for Enceladus. We test ice shell thicknesses in the range from 6 to 80 km. Several values for the potential Love number and crust viscosity are considered to reproduce the observed libration amplitude.

## 4 RESULTS

### 4.1 Libration amplitude

First we analyze how the size of the mantle affects the amplitude of longitudinal libration of the mantle and of the Tisserand frame. We apply our model to Enceladus with potential Love number  $k_2 = 0.011$  and mantle viscosity  $\eta = 10^{14}$  Pa · s to obtain the libration dependence on the ice shell thickness. In Figure 4 we observe a very large

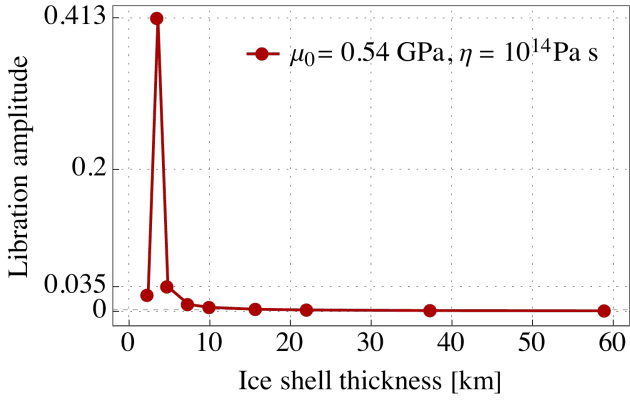


**Figure 4.** Amplitude of Enceladus’s longitudinal libration as a function of ice shell thickness.

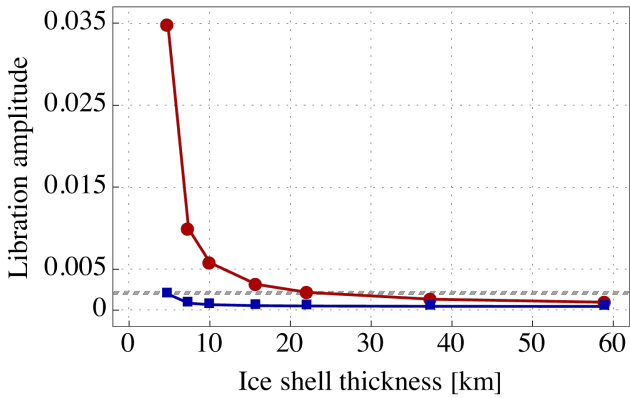


**Figure 5.** Amplitude of Enceladus’s longitudinal libration as a function of ice shell thickness. The red line with dots for stands for the shell libration and blue line with squares for the librations of bodies Tisserand frame. The hatched interval shows the measured libration amplitude with the uncertainty.

libration amplitude for a 3.6 km ice crust. This resonant behaviour is expected for models in the presence of a subsurface ocean. The presence of a subsurface ocean leads to appearance of a free libration frequency that can be resonant with the orbital frequency. This proper frequency depends on the shell thickness (Rambaux et al. 2011). The appearance of this phenomenon in our model is important since it shows that our two-layer model reproduces properties due to the presence of a subsurface ocean. Otherwise, the libration amplitude decreases with the increasing crust size, as we expected.

In Figure 5 we compare the libration of the mantle to the libration of Tisserand frame. The libration amplitude of the mean body is much smaller than the libration of the mantle and the observed libration could only be obtained for unlikely thin ice crust. We can conclude that the effective homogeneous model underestimates the libration amplitude of a body with a subsurface ocean, as in (Gevorgyan et al. 2020).

From Figure 6 we notice that the libration amplitude decreases with the increase of the prestress-elastic constant. One should not be confused with this behaviour, which is opposite to what happens with the libration dependence on the mantle rigidity, see for example (Jara-Oru e & Vermeersen 2014). The two parameters should not be confused, since one controls the elastic behaviour of the mantle and the other how much the mantle is prestressed.

From Figure 5 we can see that crust libration estimated in (Thomas et al. 2016) is obtained in our model with potential Love number of

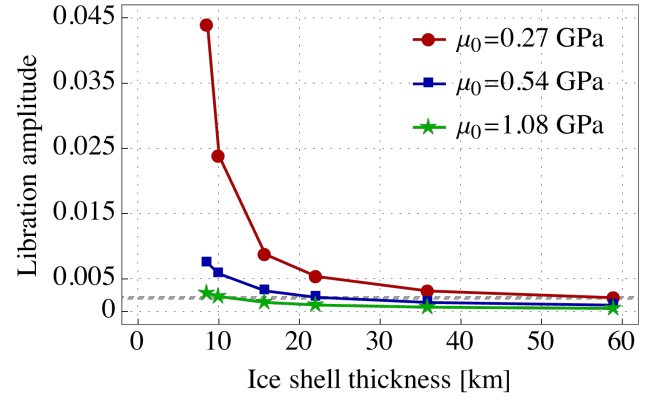


**Figure 6.** Amplitude of Enceladus’s longitudinal libration as a function of ice shell thickness for three values of the prestress-elastic constant.

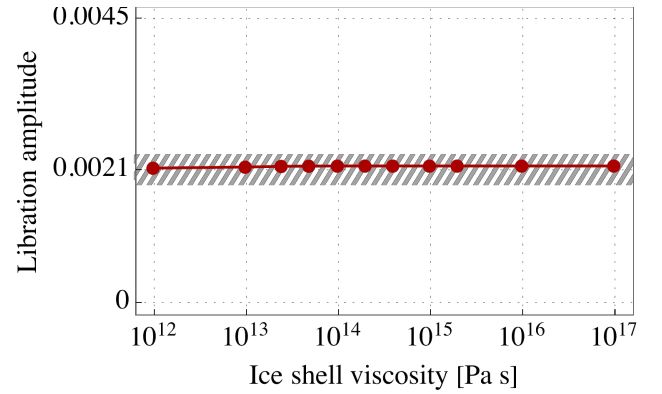


**Figure 7.** Amplitude of Enceladus’s longitudinal libration as a function of ice shell viscosity.

around 0.011, ice shell viscosity of  $10^{14}$  Pa · s and ice shell thickness of around 22 km. The viscosity of  $10^{14}$  Pa · s is usually accepted for thin ice layer at melting point in contact with the ocean (Sou cek et al. 2019). Mean viscosity of one layer ice should be much larger than the viscosity of the base layer, otherwise the dissipation in the crust will be overestimated (Rhoden & Walker 2022). From Figure 7 we can see that viscosity values in the interval  $10^{12} - 10^{17}$  Pa · s do not affect the libration amplitude, hence any value in the interval would give the same libration amplitude for the crust of Enceladus. The viscosity in this case should be constrained from the dissipation in the crust.

The prestress of Mimas dominates the forced librations of the crust and variation of parameters like viscosity and potential Love number can affect the amplitude of librations very little. The libration amplitude can be used here to constraint the first order gravitational coefficients. First we use first order gravitational coefficients  $J_2 = 0.01875$  and  $C_{22} = 0.0045$ , the potential Love number  $k_2 = 0.01$  (equivalent to  $\mu_0 = 2 \times 10^8$  Pa), and the viscosity  $\eta = 10^{15}$  Pa · s estimated in (Lainey et al. 2024). With this model parameters the observed libration is obtained for an ice shell of  $\sim 34.5$  km, the value that does not fall in the range constrained for the shell thickness in (Tajeddine et al. 2014). Observed libration of Mimas is obtained for a reasonable shell thickness if we maintain the Love number and the viscosity, but set the prestress of the shell at about 80% of the value that it would have for the gravitational coefficients in (Lainey et al. 2024). Solving Equation (11) for the new prestress we obtain gravitational coefficients in Table 1. With this parameters we

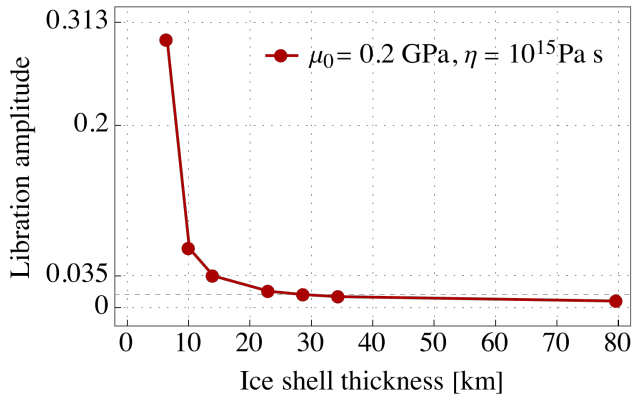


**Figure 8.** Amplitude of Mimas's longitudinal libration as a function of ice shell thickness.

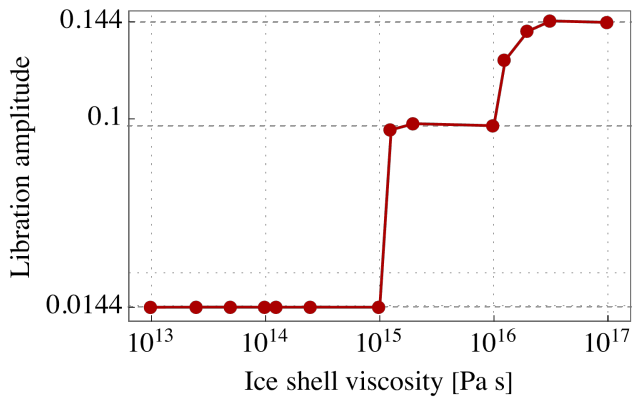


**Figure 9.** Amplitude of Mimas's longitudinal libration as a function of ice shell viscosity.

obtain measured longitudinal libration of Mimas for crust thickness of  $\sim 28$  km, see Figure 8. This value is in a good agreement with the interval constrained in (Tajeddine et al. 2014). The same crust size was obtained for Love number values in the interval  $0.00057 - 0.01$  and viscosity values in the interval  $10^{13} - 10^{15}$  Pa  $\cdot$  s. For viscosity larger than  $10^{15}$  Pa  $\cdot$  s the libration amplitude behaves as expected and increases in a ladder-like manner with increasing viscosity (Jara-Oru & Vermeersen 2014), see Figure 9.

## 4.2 Dissipation

Here we estimate the amount of energy dissipated in the mantle and on the core mantle boundary of the moons with our model. The contribution from the dissipation of the CMB is orders of magnitude smaller than the dissipation of the mantle. Our model does not account for possible dissipation in the core, hence dissipation rates in Figures 10, 11 and 12 do not represent total energy balance for the body. We do not address the problem of subsurface ocean maintenance in this paper.

From Figure 10 one can see that the dissipation in the mantle decreases with increasing  $\mu_0$ , hence with increasing potential Love number. The same behaviour is observed for the librations of the mantle, this means that once the librations is fixed in our model potential Love number should be fixed as well. We conclude that the parameter responsible for dissipation variation for a fixed mantle libration amplitude is the viscosity of the shell. From Figure 11 one can see that the dissipation rate decreases with increasing ice shell

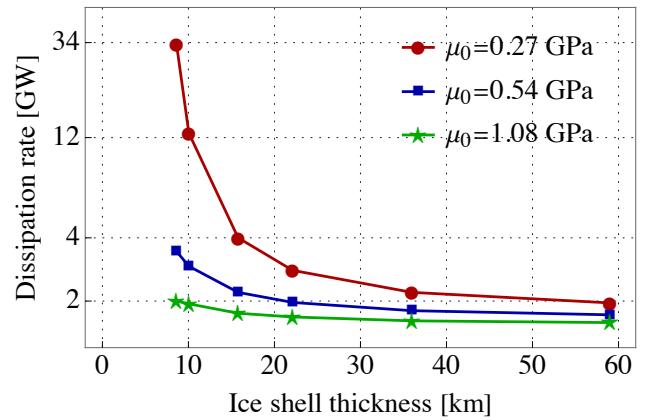


**Figure 10.** Enceladus's dissipation as a function of ice shell thickness.

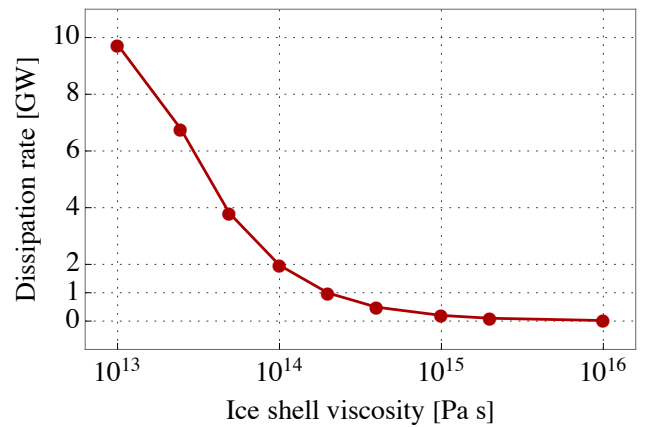


**Figure 11.** Enceladus's dissipation as a function of ice shell viscosity with  $\mu_0 = 0.54$  GPa and ice shell thickness of 22 km.

viscosity. Above results are coherent with others models in literature. If we assume shell viscosity  $\eta = 10^{14}$  Pa  $\cdot$  s tidal dissipation in the mantle of Enceladus is around 2.2 GW. The obtained value is a loose upper limit for mantle dissipation with our model and Maxwell rheology, in the absence of resonances. Other rheologies, as for example Burgers, Andrade or Sundberg–Cooper, can be easily considered in our model, and this could increase the dissipation in the mantle (Gevorgyan et al. 2020; Gevorgyan 2021; Gevorgyan et al. 2023).

In Figure 12 we plot the dissipation rate of Mimas shell and CMB against viscosity. The dissipation rate decreases with the increase of the ice shell viscosity, for the constant libration amplitude plateaus in Figure 9, and increases abruptly as the libration amplitude goes from one plateau to the next one. The dissipation rate in the mantle and CMB is around 2.17 GW for a 28 km ice shell with  $\mu_0 = 0.2$  GPa and  $\eta = 10^{15}$  Pa  $\cdot$  s viscosity. The dissipation is similar to the one of Enceladus, hence possible difference in energy balance of the two moons should come from some energy sources not considered here.

## 5 CONCLUSIONS

We show that the two layered rheological model proposed here is a good approximation for an icy moon with a global subsurface ocean if we are interested in modelling the forced longitudinal librations of the body. The model is simple and easy to implement, and it

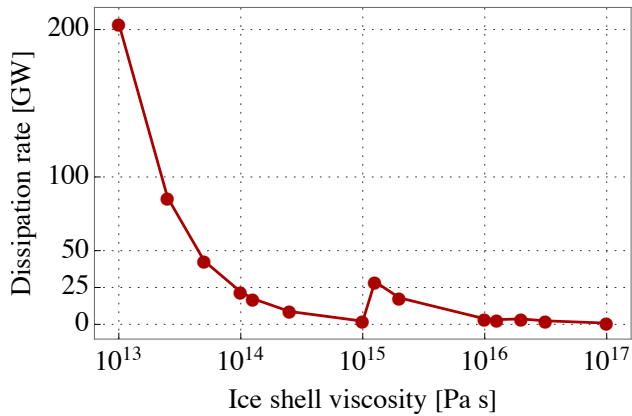


**Figure 12.** Mimas’s dissipation as a function of ice shell viscosity with  $\mu_0 = 0.2\text{GPa}$  and ice shell of 28km.

preserves well physical behaviour of a body in the presence of a global subsurface ocean, which makes it a good candidate for first quick analyses of the interior of a celestial body with measured forced librations. It can be used to check for a subsurface ocean and also to estimate the thickness of the body crust from the measured libration amplitude. The model can be extended to latitudinal librations as in (Ragazzo et al. 2022). Although simple, the model is reasonably realistic and even predicts the resonances in dissipation rate and libration amplitude as expected for bodies with global subsurface oceans (Rambaux et al. 2011).

To illustrate the behaviour of the model, we applied it to the moons of Saturn, Enceladus and Mimas, and investigated how the libration amplitude depends on the thickness and viscosity of the crust, and on the prestress of the body. The estimates for the size of the shell are in good agreement with the values in the literature. The model produces reasonable estimates for the dissipation of the mantle, but disregards the dissipation in the core. We conclude that our model is a good approximation for both Enceladus and Mimas, but lacks an energy source in the core to equilibrate the energy balance of the moons.

## ACKNOWLEDGEMENTS

The author thanks Clodoaldo Ragazzo (IME/USP) for valuable discussions during the preparation of the manuscript. The author also thanks Professor Diogo A. Gomes and the KAUST, KSA, for their kind support. This work was partially supported by FAPESP under grants 2019/25356-9 and 2021/09679-2.

## DATA AVAILABILITY

The data underlying this paper will be shared on reasonable request to the corresponding author.

## REFERENCES

- Bagheri A., et al., 2022, *Advances in Geophysics*, 63, 231  
 Beuthe M., Rivoldini A., Trinh A., 2016, *Geophys. Res. Lett.*, 43, 10,088  
 Běhouňková M., Tobie G., Čadek O., Choblet G., Porco C., Nimmo F., 2015, *Nature Geoscience*, 8, 601  
 Correia A. C. M., Ragazzo C., Ruiz L. S., 2018, *Celestial Mechanics and Dynamical Astronomy*, 130, 51

- Dmitrovskii A. A., Khan A., Boehm C., Bagheri A., van Driel M., 2022, *Icarus*, 372, 114714  
 Dziewonski A. M., Anderson D. L., 1981, *Physics of the Earth and Planetary Interiors*, 25, 297  
 Efroimsky M., 2018, *Icarus*, 300, 223  
 Ermakov A. I., et al., 2021, *The Planetary Science Journal*, 2, 157  
 Garcia R. F., et al., 2019, *Space Sci. Rev.*, 215, 50  
 Gevorgyan Y., 2021, *A&A*, 650, A141  
 Gevorgyan Y., Boué G., Ragazzo C., Ruiz L. S., Correia A. C. M., 2020, *Icarus*, 343, 113610  
 Gevorgyan Y., Matsuyama I., Ragazzo C., 2023, *MNRAS*, 523, 1822  
 Gyalay S., Nimmo F., 2022, in AGU Fall Meeting Abstracts. pp P43B–05  
 Hairer E., Nørsett S. P., G. W., 1993, *Solving Ordinary Differential Equations* I. Springer  
 Iess L., et al., 2014, *Science*, 344, 78  
 Jara-Orué H. M., Vermeersen B. L. A., 2014, *Icarus*, 229, 31  
 Kang W., Mittal T., Bire S., Campin J.-M., Marshall J., 2022, *Science Advances*, 8, eabm4665  
 Khan A., Pommier A., Neumann G. A., Mosegaard K., 2013, *Tectonophysics*, 609, 331  
 Khan A., et al., 2021, *Science*, 373, 434  
 Lainey V., Rambaux N., Tobie G., Cooper N., Zhang Q., Noyelles B., Baillié K., 2024, *Nature*, 626, 280  
 Matsumoto K., Yamada R., Kikuchi F., Kamata S., Ishihara Y., Iwata T., Hanada H., Sasaki S., 2015, *Geophys. Res. Lett.*, 42, 7351  
 Nadezhdina I. E., Zubarev A. E., Brusnikin E. S., Oberst J., 2016, *ISPRS - International Archives of the Photogrammetry, Remote Sensing and Spatial Information Sciences*, 41B4, 459  
 Nimmo F., Pappalardo R. T., 2016, *Journal of Geophysical Research (Planets)*, 121, 1378  
 Peale S. J., Margot J.-L., Hauck S. A., Solomon S. C., 2014, *Icarus*, 231, 206  
 Ragazzo C., 2020, *São Paulo Journal of Mathematical Sciences*, 14, 1  
 Ragazzo C., Ruiz L. S., 2017, *Celestial Mechanics and Dynamical Astronomy*, 128, 19  
 Ragazzo C., Boué G., Gevorgyan Y., Ruiz L. S., 2022, *Celestial Mechanics and Dynamical Astronomy*, 134, 10  
 Rambaux N., van Hoolst T., Karatekin Ö., 2011, *A&A*, 527, A118  
 Rambaux N., Castillo-Rogez J. C., Le Maistre S., Rosenblatt P., 2012, *A&A*, 548, A14  
 Rhoden A. R., Walker M. E., 2022, *Icarus*, 376, 114872  
 Souček O., Běhouňková M., Čadek O., Hron J., Tobie G., Choblet G., 2019, *Icarus*, 328, 218  
 Tajeddine R., Rambaux N., Lainey V., Charnoz S., Richard A., Rivoldini A., Noyelles B., 2014, *Science*, 346, 322  
 Thomas P. C., Tajeddine R., Tiscareno M. S., Burns J. A., Joseph J., Loredó T. J., Helfenstein P., Porco C., 2016, *Icarus*, 264, 37  
 Tiscareno M. S., Thomas P. C., Burns J. A., 2009, *Icarus*, 204, 254  
 Tromp J., 2020, *Nature Reviews Earth and Environment*, 1, 40  
 Vance S. D., et al., 2018, *Journal of Geophysical Research (Planets)*, 123, 180

This paper has been typeset from a  $\text{\TeX}/\text{\LaTeX}$  file prepared by the author.